Inorganic Chemistry

Article

pubs.acs.org/IC

Synthesis, Structure, and Transport Properties of Type-I Derived Clathrate $Ge_{46-x}P_xSe_{8-y}$ (x = 15.4(1); y = 0−2.65) with Diverse Host−Guest Bonding

Maria A. Kirsanova,[†] Takao Mori,[‡] Satofumi Maruyama,[‡] Maria Matveeva,[§] Dmitry Batuk,[§] Artem M. Abakumov,[§] Andrei V. Gerasimenko,[⊥] Andrei V. Olenev,[¶,#] Yuri Grin,[&] and Andrei V. Shevelkov*[,†]

[†]Department of Chemistry, Lomonosov Moscow State University, 119991 Moscow, Russia

[‡]International Center for Materials Nanoarchitectonics (MANA), National Institute for Materials Science (NIMS), 305-0044 Tsukuba, Japan

[§]EMAT, University of Antwerp, Groenenborgerlaan 171, B-2020 Antwerp, Belgium

[⊥]Institute of Chemistry, FEB RAS, 690022 Vladivostok, Russia

[¶]"SineTheta" Ltd., Scientific Park of Lomonosov Moscow State University, 119991 Moscow, Russia

[&]Max-Planck-Institut für Chemische Physik fester Stoffe, Dresden, Germany

Supporting Information

ABSTRACT: A first clathrate compound with selenium guest atoms, $[Ge_{46-x}P_x]Se_{8-y}\square_y$ (x = 15.4(1); y = 0−2.65; □ denotes a vacancy), was synthesized as a single-phase and structurally characterized. It crystallizes in the space group $Fm\bar{3}$ with the unit cell parameter a varying from 20.310(2) to 20.406(2) Å and corresponding to a 2 × 2 × 2 supercell of a usual clathrate-I structure. The superstructure is formed due to the symmetrical arrangement of the three-bonded framework atoms appearing as a result of the framework transformation of the parent clathrate-I structure. Selenium guest atoms occupy two types of polyhedral cages inside the positively charged framework; all selenium atoms in the larger cages form a single covalent bond with the framework atoms, relating the title compounds to a scanty family of semiclathrates. According to the measurements of electrical resistivity and Seebeck coefficient, $[Ge_{46-x}P_x]Se_{8-y}\square_y$ is an n-type semiconductor with E_g = 0.41 eV for x = 15.4(1) and y = 0; it demonstrates the maximal thermoelectric power factor of 2.3 × 10^{-5} W K^{-2} m^{-1} at 660 K.

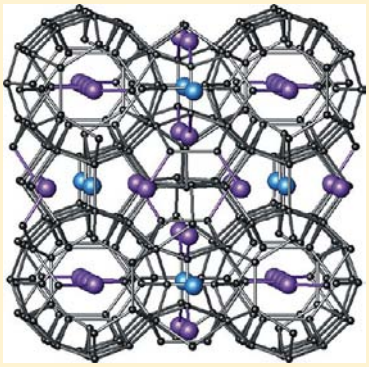

INTRODUCTION

Clathrates have been known for over 200 years. Their first representatives were hydrates of various gases and liquids, among which was the famous chlorine hydrate discovered by Davy.[1] The discovery of sodium silicide Na_8Si_{46}[2] in the 1960s led the way to the era of intermetallic and semiconducting clathrates. Interest in clathrates has grown rapidly due to development of the "phonon glass−electron crystal" concept,[3] according to which compounds with the cage structure, including clathrates, are promising thermoelectric materials. Indeed, certain clathrates demonstrate encouraging values of the thermoelectric figure of merit ZT. For example, $Ba_8Ge_{30}Ga_{16}$ exhibits ZT > 1 at temperatures higher than 800 K.[4] A wide variety of other intriguing physical properties, such as superconductivity in $Ba_{8-x}Si_{46}$[5] or ferromagnetism in $Eu_8Ga_{16}Ge_{30}$[6] and $Ba_8Mn_2Ge_{44}$,[7] were revealed for clathrates. More than 250 binary, ternary, and quaternary compounds of various clathrate types have been synthesized and surveyed up to now.[8]

Though several clathrate structure types have been documented in the literature,[1,9] the vast majority of intermetallic/semiconducting clathrates belong to the clathrate-I structure type, and most compounds of the clathrate-I structure crystallize in the cubic space group $Pm\bar{3}n$. Their crystal structure features a three-dimensional host framework, based on the group 14 elements, encapsulating guest atoms in large cavities. Strong covalent bonds exist within the framework, whereas the guest atoms are held within the framework cavities by weaker interactions. In most clathrates the electron balance between host and guest substructures could be explained in terms of the Zintl concept.[10] It implies that electronegative atoms accept electrons from more electropositive atoms to form two-center, two-electron bonds and (if necessary) lone pairs, thus completing their 8-electron shell. According to this concept, two types of clathrates can be distinguished. Most abundant anionic clathrates have a negatively charged framework trapping cations of alkali or alkali-earth metals or europium. There also exists a scanty group of clathrate-I compounds with the inversed polarity

Received: May 25, 2012
Published: December 31, 2012

   dx.doi.org/10.1021/ic3011025 | *Inorg. Chem.* 2013, 52, 577−588

known as cationic clathrates. Their framework is positively charged and traps halides or tellurium anions in its cages. A family of germanium-based cationic clathrates $[Ge_{38}Pn_8]X_8$ (Pn = P, As, Sb; X = Cl, Br, I) was first discovered by Menke and von Schnering in the early 1970s.[11] Later a number of tin[12] and silicon[13,14] based clathrates were synthesized. Most of them have halide anions inside the framework cavities, and there are just a few examples of clathrates-I with tellurium as guest atoms reported in the literature: $Si_{46-x}P_xTe_y$,[14] $Si_{38}Te_{16}$,[15] $Ge_{30}P_{16}Te_8$,[16] and $Ge_{46-x}P_xTe_y$,[17] the latter being in fact a semiclathrate as part of guest atoms form a single covalent bond with the framework. Up to now, no selenium analogues were reported.

In this work, we report the first example of a clathrate-I compound containing selenium as guest atoms. We show that $[Ge_{46-x}P_x]Se_{8-y}\square_y$ (x = 15.4(1); y = 0–2.65; $\square$ denotes a vacancy) possesses a rare type of clathrate-I superstructure and belongs to a small family of semiclathrates. We report on its electronic structure, emphasizing the details of the host–guest bonding, and also present its transport properties as part of a search for new clathrate-based thermoelectric materials.

EXPERIMENTAL SECTION

1. Synthesis and Sample Characterization. The samples in the Ge–P–Se system were prepared from the following starting materials: Ge powder (Aldrich, 99.999%), Se powder (Aldrich, 99.99%), and red P powder (Sigma-Aldrich, 97%). Red phosphorus was purified by a standard method reported elsewhere.[18] Elementary substances were mixed (0.5–1.0 g total weight), ground in an agate mortar, and sealed in silica ampules under dynamic vacuum. Synthesis was performed for several compositions, corresponding to the common formulas $[Ge_{46-x}P_x]Se_y$, where x was varied from 14 to 17 and y was varied from 5 to 8. Synthesis was carried out with different temperatures between 853 and 973 K to determine the optimal conditions. The final products were obtained by utilizing a two-step annealing. Ampules with starting materials were placed into a furnace, heated to 873 K in 12 h, annealed at this temperature for 72 h, and cooled to room temperature in the furnace. The obtained powders were reground, sealed in silica ampules, and annealed under the same conditions for other 120 h.

The obtained powders were investigated by X-ray powder diffraction (XRD), using a STADI-P (Stoe) diffractometer (Cu Kα_1, λ = 1.5406 Å) at room temperature. The unit cell parameters were calculated from least-squares fits with use of Ge (a = 5.6576 Å) as an internal standard utilizing the WINXPOW program package.

Differential scanning calorimetry (DSC) measurements were carried out with a precalibrated STA 449 F1 Jupiter apparatus (Netzsch). About 10 mg of the title compound was placed in an alumina crucible and tightly closed with an alumina cap. The sample was heated to 1273 K in dry argon flow at a ramp rate of 10 deg min^{-1}. The Proteus Thermal Analysis program (Netzsch) was used for the data processing and analyzing.

For the energy-dispersive X-ray (EDX) analysis, a JEOL JSM-6490LV scanning electron microscope operating at 30 kV and equipped with an Oxford Instruments detector system was used. Polished pellets or single crystals were attached so as to achieve the orientation of a sample as parallel to the support as possible. The data were collected for 6 points for crystals or 10 points for pellets and then averaged.

2. Single Crystal X-ray Diffraction Study. From the samples obtained at different temperatures between 843 and 973 K small, well-shaped crystals were selected. Several crystals were tested and two of them selected for the complete structural analysis.

The crystal structure of the crystal **I** was determined by using the single crystal X-ray diffraction data collected by means of a CAD-4 (NONIUS) diffractometer (Mo Kα) at room temperature. The unit cell parameters were refined on the basis of 24 well-centered reflections in the angular range of 15° < θ < 17° and agreed well with those found from the powder data. The data were collected at room temperature and corrected for polarization and Lorenz effects. A semiempirical absorption correction was applied to the data based on azimuthal scans of 9 reflections having their χ angles close to 90°. X-ray diffraction measurements for crystal **II** were performed with a Bruker APEX II CCD diffractometer at 293 and 173 K. The unit cell parameter was refined by using a full set of reflections collected in the range of 2° < θ < 35° and 2° < θ < 45°, respectively. A multiscan absorption correction was utilized.

The data were processed with use of the SHELX-97 package;[19] the crystal structure was solved by direct methods and refined by full-matrix least-squares fits on F^2 in an anisotropic approximation for all atoms. Important crystallographical information is collected in Tables 1 and 2. Further details on the crystal structure investigation may be obtained from the Fachinformationszentrum Karlsruhe, D-76344 Eggenstein-Leopoldshafen, Germany (fax: +(49)7247-808-666; e-mail: crysdata@fiz-karlsruhe.de), reference numbers CSD-424302 (**I**), CSD-424303 (**II** at 293 K), and CSD-424332 (**II** at 173 K).

Table 1. Data Collection and Structure Refinement Parameters for $[Ge_{46-x}P_x]Se_{8-y}\square_y$

	I	**II**	**II** (173 K)
refined composition	$Ge_{30.71(11)}P_{15.29(11)}Se_{5.38(4)}$	$Ge_{30.54(6)}P_{15.46(6)}Se_{7.970(10)}$	$Ge_{30.70(5)}P_{15.30(5)}Se_{7.970(4)}$
space group	$Fm\bar{3}$		
M_r [g mol^{-1}]	3127.23	3321.07	3331.82
cell parameters [Å]	20.310(2)	20.406(2)	20.351(2)
V [Å^3]	8377.3(16)	8496.8(17)	8429.3(16)
T [K]	293(2)	293(2)	173(2)
Z	8		
radiation, λ [Å]	Mo Kα, 0.71073		
ρ_{calcd} [g·cm^{-3}]	4.959	5.192	5.251
μ [mm^{-1}]	26.918	28.594	28.992
θ range [deg]	3.33 < θ < 27.92	2.00 < θ < 35.06	1.73 < θ < 45.21
reflns collected/ unique	2752/918 [R(int) = 0.0440]	8498/1683 [R(int) = 0.0418]	39918/3101 [R(int) = 0.0623]
data/ parameter	918/59	1683/57	3101/58
R_1, $wR_2[I > 2\sigma(I)]$	0.0344, 0.0628	0.0254, 0.0681	0.0290, 0.0541
goodness-of-fit on F^2	1.063	1.112	1.099

3. Electron Microscopy. The sample with the composition $Ge_{30.6}P_{15.4}Se_8$ was prepared for the electron microscopy investigation by grinding the powder in an agate mortar in ethanol and depositing drops of suspension onto holey carbon grids. Selected area electron diffraction (SAED) observations were performed with a Philips CM20 electron microscope; high-angle annular dark field scanning transmission electron microscopy (HAADF-STEM) observations were performed with a FEI Tecnai G2 electron microscope operated at 200 kV. The HAADF-STEM image simulation from the structure data was done with QSTEM2.10 software[20] assuming the crystal thickness of 5 nm.

4. Band Structure Calculations. Electronic structure calculation and analysis of chemical bonding were carried out for the ordered model with the composition $Ge_{32}P_{14}Se_8$. The atomic coordinates were taken from structure **II** (see Table 2) with full occupation of the positions as follows: Se1, Se2, Se3, Se4, Ge1, Ge2, Ge3, P4, P5, Ge6, Ge7, P8. The TB-LMTO-ASA program package was used.[21] The Barth–Hedin exchange potential[22] was employed for the local density approximation (LDA) calculations. The radial scalar-relativistic Dirac equation was solved to obtain the partial waves. Despite the calculation within the atomic sphere approximation (ASA) which includes

dx.doi.org/10.1021/ic3011025 | Inorg. Chem. 2013, 52, 577–588

Table 2. Atomic Coordinates, Site Occupancy, and Equivalent Isotropic Displacement Parameter (Å^2) for $[Ge_{46-x}P_x]Se_{8-y}\square_y$ in the Space Group $Fm\bar{3}$

atom	Wyckoff	occupancy	x	y	z	U_{eq}, Å^2
$Ge_{30.71(11)}P_{15.29(11)}Se_{5.38(4)}$ (structure **I**)						
Se(1)	4*a*	0.826(19)	0	0	0	0.021(2)
Se(2)	4*b*	0.823(19)	0	0.5	0	0.017(2)
Se(3)	8*c*	1	0.25	0.25	0.25	0.024(1)
Se(4)	48*h*	0.592(2)	0.2491(1)	0.1208(1)	0.5	0.017(1)
Ge(1)	96*i*	1	0.7497(1)	0.4080(1)	0.1900(1)	0.008(1)
Ge(2)	48*h*	1	0.5	0.4394(1)	0.1581(1)	0.010(1)
Ge(3)	48*h*	1	0	0.3434(1)	0.0606(1)	0.008(1)
E(4)[a]	48*h*	0/1	0.5	0.3784(1)	0.2571(1)	0.006(1)
E(5)	32*f*	0.165/0.835(7)	0.9082(1)	0.4082(1)	0.0918(1)	0.008(1)
E(6)	32*f*	0.699/0.301(7)	0.8419(1)	0.3419(1)	0.1581(1)	0.010(1)
E(7)	32*f*	0.490/0.510(7)	0.6578(1)	0.3422(1)	0.1578(1)	0.011(1)
E(8)	32*f*	0.323/0.677(7)	0.5921(1)	0.4079(1)	0.0921(1)	0.007(1)
$Ge_{30.4(2)}P_{15.6(2)}Se_{7.970(10)}$ (structure **II** at 293 K)						
Se(1)	4*a*	0.984(10)	0	0	0	0.008(1)
Se(2)	4*b*	0.945(10)	0.5	0	0	0.010(1)
Se(3)	8*c*	1	0.25	0.25	0.75	0.008(1)
Se(4)	48*h*	1	0.2510(1)	0	0.8780(1)	0.008(1)
Ge(1)	96*i*	1	0.2504(1)	0.8100(1)	0.0923(1)	0.003(1)
Ge(2)	48*h*	1	0.3423(1)	0.9394(1)	0	0.004(1)
Ge(3)	48*h*	1	0.1551(1)	0	0.9399(1)	0.003(1)
E(4)[a]	48*h*	0.048/0.952(2)	0.2437(1)	0.8781(1)	0	0.003(1)
E(5)	32*f*	0.180/0.820(3)	0.0922(1)	0.9079(1)	0.9079(1)	0.001(1)
E(6)	32*f*	0.637/0.363(3)	0.1583(1)	0.8417(1)	0.8417(1)	0.002(1)
E(7)	32*f*	0.410/0.590(3)	0.3423(1)	0.8423(1)	0.8423(1)	0.002(1)
E(8)	32*f*	0.314/0.686(3)	0.4077(1)	0.9077(1)	0.0923(1)	0.002(1)
$Ge_{30.70(5)}P_{15.30(5)}Se_{7.970(4)}$ (structure **II** at 173 K)						
Se(1)	4*a*	1	0	0	0	0.006(1)
Se(2)	4*b*	0.939(9)	0.5	0	0	0.007(1)
Se(3)	8*c*	1	0.25	0.25	0.75	0.005(1)
Se(4)	48*h*	1	0.2510(1)	0	0.8781(1)	0.005(1)
Ge(1)	96*i*	1	0.2504(1)	0.8099(1)	0.0923(1)	0.001(1)
Ge(2)	48*h*	1	0.3423(1)	0.9393(1)	0	0.002(1)
Ge(3)	48*h*	1	0.1551(1)	0	0.9399(1)	0.001(1)
E(4)[a]	48*h*	0.054/0.946(2)	0.2437(1)	0.8782(1)	0	0.002(1)
E(5)	32*f*	0.184/0.816(2)	0.0922(1)	0.9078(1)	0.9078(1)	0.001(1)
E(6)	32*f*	0.653/0.347(2)	0.1582(1)	0.8418(1)	0.8418(1)	0.001(1)
E(7)	32*f*	0.431/0.569(2)	0.3422(1)	0.8422(1)	0.8422(1)	0.002(1)
E(8)	32*f*	0.323/0.677(2)	0.4077(1)	0.9077(1)	0.0923(1)	0.001(1)

[a]E4 = *sof*(Ge4)/*sof*(P4); E5 = *sof*(Ge5)/*sof*(P5); E6 = *sof*(Ge6)/*sof*(P6); E7 = *sof*(Ge7)/*sof*(P7); E8 = *sof*(Ge8)/*sof*(P8).

corrections for the neglect of interstitial regions and partial waves of higher order,[23] addition of empty spheres was necessary. The following radii of the atomic spheres were applied for the calculations: r(Se1) = 2.369 Å, r(Se2) = 2.387 Å, r(Se3) = 2.352 Å, r(Se4) = 1.332 Å, r(Ge1) = 1.338 Å, r(Ge2) = 1.366 Å, r(Ge3) = 1.309 Å, r(P4) = 1.321 Å, r(P5) = 1.325 Å, r(Ge6) = 1.312 Å, r(Ge7) = 1.312 Å, r(P8) = 1.325 Å. For the calculation a basis set containing Se(4*s*,4*p*,4*f*) for Se1−3 or Se(4*s*,4*p*) for Se4, Ge(4*s*,4*p*), and P(3*s*,3*p*) states was employed for a self-consistent calculation with Se(4*d*) for Se1−3, Ge(4*d*), and P(3*d*) functions being down-folded. The electron localizability indicator (ELI, Y) was evaluated in the ELI-D representation according to ref 24 with an ELI-D module within the program package TB−LMTO−ASA.[21] Topological analysis of the electron density, i.e., estimation of the shapes, volumes, and charges of the atoms after Bader (QTAIM atoms[25]), and of the electron localizability indicator were performed with the program DGrid.[26]

5. Physical Property Measurements. Resistivity and thermoelectric power measurements were performed with an ULVAC ZEM-2 in a helium atmosphere by using the four-probe and differential method, respectively. The temperature range of measurements was from 300 to 673 K. The powder of the clathrate phase with unit cell parameter a = 20.410(2) Å, corresponding to the composition $Ge_{30.6(1)}P_{15.4}Se_8$, was sintered by spark plasma sintering (SPS) at a pressure of 60 MPa and a temperature of 773 K in an argon atmosphere with use of LABOX-625 (SINTER LAND). A rectangular-shaped sample (1.5 mm × 4.5 mm × 9.1 mm) with the density of 4.90 g cm^{-3} (94−95% of the theoretical density) was cut from the SPS-prepared product and used for measurements. It was clutched between nickel contacts; the thermocouple was attached to one of the perpendicular sides. The rest of the sample was used for the XRD and energy-dispersive X-ray (EDX) analysis. The XRD analysis confirmed that the sample was pure $Ge_{30.6(1)}P_{15.4}Se_8$ compound with the unit cell parameter a = 20.410(2) Å. EDX analysis was performed to confirm that the composition of the sample did not change in the course of SPS-compacting: found Ge:P:Se, 54(3):32(4):14(2); calculated from the X-ray crystal structure data, 56.6(4):28.5(4):14.8(1).

RESULTS AND DISCUSSION

1. Synthesis and Phase Composition. Synthesis of the $[Ge_{46-x}P_x]Se_{8-y}$ samples was undertaken for different values of

dx.doi.org/10.1021/ic3011025 | *Inorg. Chem.* 2013, 52, 577−588

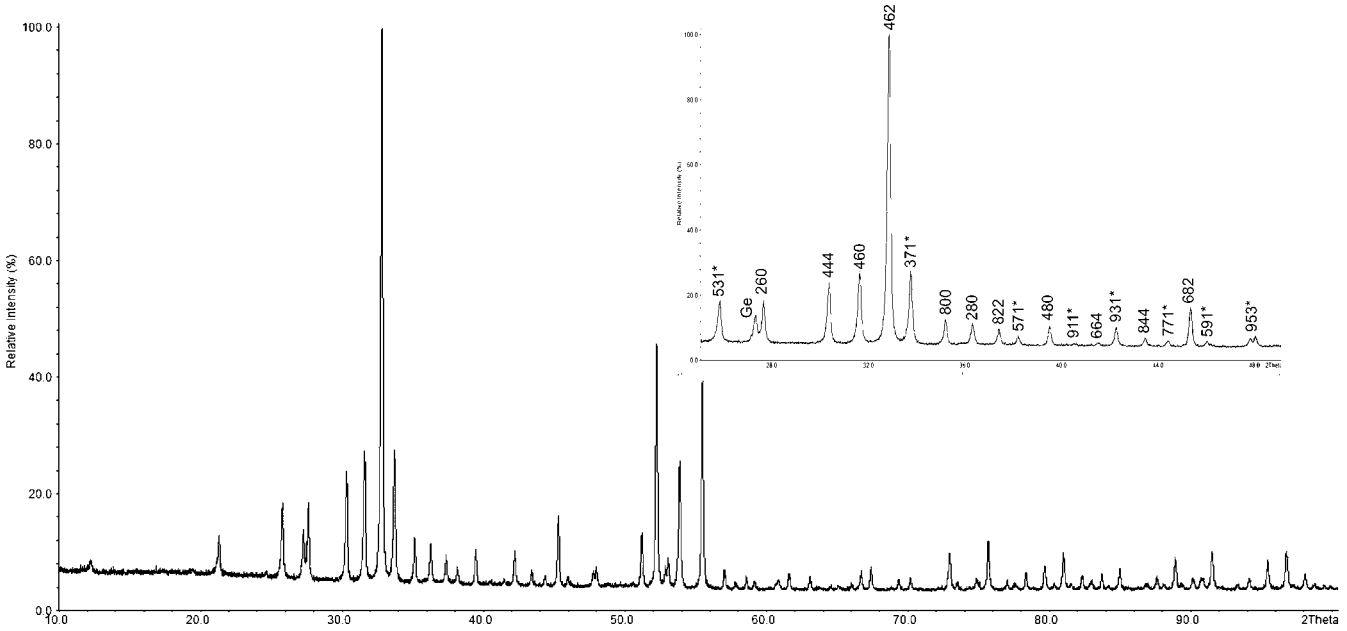

Figure 1. XRD pattern of $Ge_{30.6}P_{15.4}Se_8$ (structure **II**), Cu Kα_1 radiation. The zoomed area shows a fragment of the pattern including the characteristic peaks (marked with an asterisk), which are not observed in a primitive cubic cell with $a_P = a_F/2$, typical of type-I clathrates.

x and y. A single-phase sample was prepared only for the composition with the maximum content of selenium ($y = 0$) and $x = 15.4(1)$. The XRD pattern for $Ge_{30.6}P_{15.4}Se_8$ showed no admixtures and was indexed in a cubic F-centered cell with the unit cell parameter $a = 20.410(2)$ Å (Figure 1). The composition was further confirmed by the X-ray crystal structure refinement and EDX analysis. Upon keeping the Ge/P ratio corresponding to the $[Ge_{30.6}P_{15.4}]$ formula and decreasing the amount of selenium from $y = 0$ to $y = 2.6$, we observed the formation of the clathrate phase with the unit cell parameter a decreasing from 20.410(3) to 20.315(3) Å; however, in all cases the product was contaminated by a small amount of side phases. Altering the Ge/P ratio always led to a noticeable increase in the amount of impurities. Single crystals of the title clathrates were selected from the samples with different starting compositions but always showed the same x value according to the crystal structure refinement (see below). Analyzing all these data and taking into account the accuracy of the composition determination we conclude that $[Ge_{46-x}P_x]Se_{8-y}$ exists for $x = 15.4(1)$ and y varying from 0 to ~2.65.

It should be noted that the results of the DSC measurements indicate that the decomposition of the sample starts at 800 K under argon flow. However, the synthesis was carried out in sealed ampules under conditions at which high pressure of phosphorus develops preventing the decomposition at higher temperatures and rendering the synthesis at 873 K possible.

2. Crystal Structure Solution. The solution of the crystal structure was carried out for several crystals with different unit cell parameters (a lies between 20.310(2) and 20.406(2) Å). Their composition corresponds to the general formula $[Ge_{46-x}P_x]Se_{8-y}\square_y$. The crystal structure solutions differ only slightly in the values of y and in the accuracy of determination of the atomic coordinates and site occupancies, whereas the values of x remain constant within the accuracy of determination. Two experiments (structures **I** and **II**, Table 2) with the boundary values of the unit cell parameter were selected for further analysis. All crystals with intermediate values of the unit cell parameter showed in general the same crystal structure as one with $a = 20.310(2)$ Å (structure **I**) but were refined with lower accuracy.

The crystal structures **I** and **II** were solved by direct methods, SHELXS-97,[19] in the cubic space group $Fm\bar{3}$. At the first stage, four sites (4*a*, 4*b*, 8*c*, and 48*h*) with highest electron density were assigned to selenium atoms based on supposition that among Ge, P, and Se only the latter might act as guest atoms. All remaining peaks were set as germanium. After several cycles of refinement three independent germanium sites were determined (one 96*i* and two 48*h*). Other sites, showing too high values of atomic displacement parameters (ADPs), were set as jointly occupied by germanium and phosphorus. In total, 12 sites were identified, four of which ($32f_1$–$32f_4$) were jointly populated by Ge and P. Afterward, partial occupancy for the selenium sites was checked and confirmed for some of them (see Table 2). Finally, the structure was refined with an anisotropic description of atomic displacements for all atoms. The final difference Fourier map showed no peaks of electron density higher than 1 e/Å^3.

3. Description of the Crystal Structure. A general view of the crystal structure is given in Figure 2. Compounds **I** and **II** with the common formulas $[Ge_{46-x}P_x]Se_{8-y}\square_y$ both crystallize in the cubic space group $Fm\bar{3}$ and possess a structure motive tightly related to the clathrate-I structure. Germanium and phosphorus atoms form a three-dimensional framework containing two types of polyhedral cavities: 20-vertex pentagonal dodecahedra and larger 24-vertex tetrakaidekahedra. Selenium atoms are located in the centers of those cages. If all selenium atoms were isolated, i.e., they had no covalent bonds with the framework, it would be a typical crystal structure of clathrate-I. However, in the structure of $[Ge_{46-x}P_x]Se_{8-y}\square_y$ a peculiar reconstruction of the framework takes place that forces the transformation from the space group $Pm\bar{3}n$ to $Fm\bar{3}$. A half of the 24*k*–24*k* dumbbells in the space group $Pm\bar{3}n$ rotate by 90°, breaking bonds with neighboring atoms in the 6*c* site (small black circles in Figure 3, left) and forming new bonds with guest selenium atoms (large dark gray circles in Figure 3,

dx.doi.org/10.1021/ic3011025 | Inorg. Chem. 2013, 52, 577–588

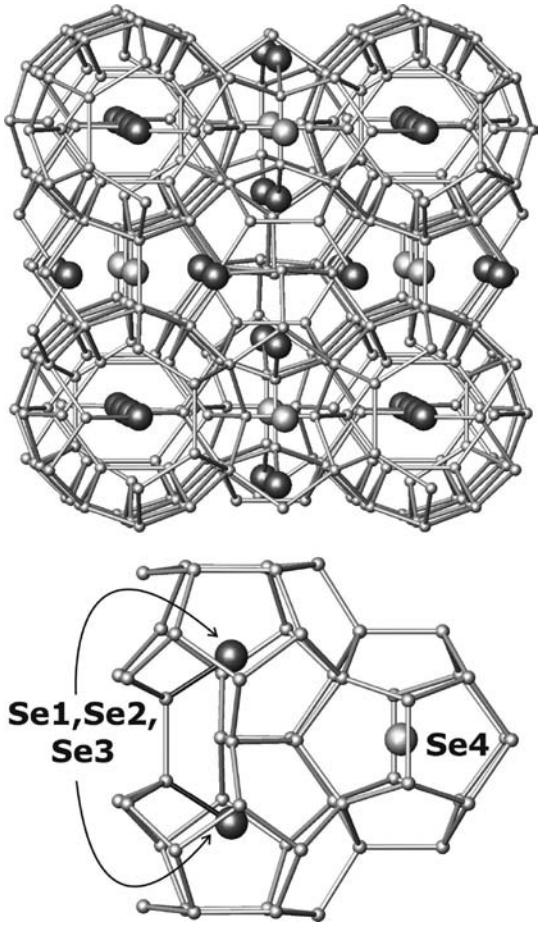

Figure 2. General view of the crystal structure of $[Ge_{46-x}P_x]Se_{8-y}\square_y$ (top) and a fragment of the structure, made up of one small and two distorted large cages filled with guest atoms (bottom).

middle). Atoms at the $48h_3$ site (small black circles) remain three-bonded.[27] In such a way a portion of the guest selenium atoms have a single covalent bond with framework atoms. Such a peculiarity allows $[Ge_{46-x}P_x]Se_{8-y}\square_y$ to be related to the family of semiclathrates. Due to the formation of the host–guest bond, 24-vertex cages become strongly distorted from one side and can no longer be described within the polyhedral model.

Upon the framework reconstruction three-bonded atoms appear in the framework. Taking in mind that all framework atoms should be four-coordinated, the three-bonded atoms might be considered as atoms having three 2c–2e bonds and a lone electron pair stretching in the fourth direction. Those lone electron pairs are arranged in such a way that the doubling of the unit cell is necessary to describe the symmetry of the crystal structure. Therefore $[Ge_{46-x}P_x]Se_{8-y}\square_y$ shows an 8-time volume increase compared to the typical clathrate-I structure and demonstrates a superstructure of clathrate-I. The same type of superstructure has been recently reported for another germanium-based semiclathrate $[Ge_{46-x}P_x]Te_y$.[17] Site splitting under transition from the space group $Pm\bar{3}n$ to its subgroup $Fm\bar{3}$ is presented in Scheme 1.

4. Crystal Structure within the Homogeneity Range. Two crystal structures with different unit cell parameters were selected for the scrutinized analysis. Tables 2 and 3 contain information about atomic coordinates, site occupancies, and selected interatomic distances. Structure **I** has the refined composition $Ge_{30.71(11)}P_{15.29(11)}Se_{5.38(4)}\square_{2.62}$, where $\square$ denotes a vacancy, and the unit cell parameter a = 20.310(2) Å. Germanium exclusively occupies three framework positions: one 96*i* and two 48*h*. Another 48*h* site is occupied by phosphorus, while the remaining four 32*f* framework sites are jointly populated by Ge and P atoms. Guest selenium atoms are located in the 20-vertex cavities with the centers at the 4*a*, 4*b*, and 8*c* sites and in the 24-vertex cavities centered at the 48*h* site. Only the 8*c* site is fully occupied by selenium, whereas other sites show partial occupancy. Selenium atoms in the $48h_4$ site form a single covalent bond with Ge3 atoms of the framework. Due to such a close distance between the host and guest larger cavities are strongly distorted from one side and could no longer be described in terms of the polyhedral presentation. Vacancies are present only in the guest positions, but there are no vacancies in the framework. That is why two types of coordination for Ge3 atoms, which form bonds with selenium atoms, are possible. If Se4 is present, Ge3 is four-bonded; if Se4 is absent (vacancy in the guest site), Ge3 is three-bonded. Thus, three-bonded atoms are present in two framework positions: in the $48h_3$ site, purely occupied by phosphorus and causing the superstructure formation, and in the $48h_2$ site in the case of a vacancy in the guest position.

Structure **II** has the refined composition $Ge_{30.54(6)}P_{15.46(6)}Se_{7.970(10)}\square_{0.03}$ and the unit cell parameter a = 20.406(2) Å. As in structure **I**, Ge atoms occupy three framework positions, but there is no site exclusively occupied by phosphorus. Five positions are jointly populated by germanium and phosphorus, though the percentage of Ge atoms in the $48h_4$ site is less than 5%. Two of four guest positions (4*a* and 4*b*) are partially occupied, but their occupancy tends to unity. In terms of such a large unit cell it might be supposed that the number of vacancies is negligibly small. The $48h_3$ site is fully occupied by the Se4 atoms having a covalent bond with the framework, opposite that of structure **I**. This is a significant difference, because all guest atoms inside the large cages are bonded to the framework. For spatial reasons the formation of a bond between the framework and guests inside the small cavities is impossible. That selenium occupies all guest positions and the host–guest bonds are formed by all guest atoms of the large cages makes structure **II** an ideal type-I semiclathrate.

Structure **II** was also refined by using the data collected at 173 K. The refined composition $Ge_{30.70(5)}P_{15.30(5)}Se_{7.970(4)}$ is the same within the 2σ as the one obtained at room temperature. There are no changes in the crystal structure with the exception of the negligible difference in the site occupancies, which falls within the standard uncertainties limit. Thermal reduction of the unit cell parameter, interatomic distances, and ADP values is observed.

The crystal structure of $[Ge_{46-x}P_x]Se_{8-y}\square_y$ closely resembles that of another semiclathrate, $[Ge_{46-x}P_x]Te_y$. However, there exists an important difference between its crystal structure and that of the title clathrate. An additional position in the framework ($48h_5$) appears in the crystal structure of $[Ge_{46-x}P_x]Te_y$ and increases in occupancy with increasing the unit cell parameter. This $48h_5$ site is responsible for the presence of isolated guest atoms in large cavities. Due to that site, isolated and bonded atoms can exist together with vacant cages. On the contrary, in the case of $[Ge_{46-x}P_x]Se_{8-y}\square_y$ neither structure **I** nor structure **II** shows any evidence of existence of an additional framework site. Thus, transformation of the usual clathrate-I structure in the semiclathrate structure takes place

dx.doi.org/10.1021/ic3011025 | *Inorg. Chem.* 2013, 52, 577–588

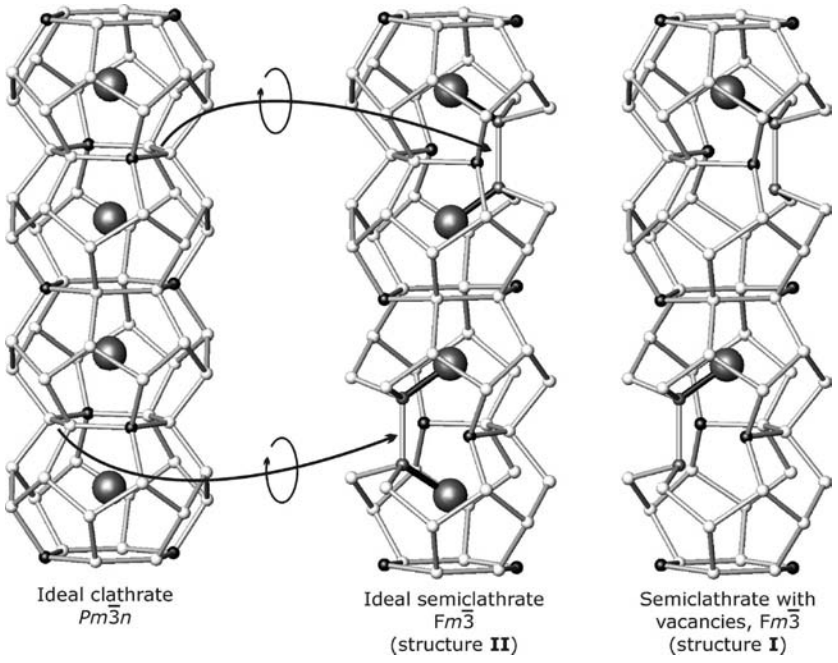

Figure 3. Transformation of the crystal structure from ideal clathrate to semiclathrate. A portion of the 24*k*−24*k* dumbbells in the ideal clathrate structure ($Pm\bar{3}n$) rotate by 90°, breaking bonds with neighboring framework atoms in the 6*c* site (small black circles, left) and forming bonds with guest atoms (large dark gray circles, middle). The 24*k* and 6*c* sites of the initial structure become the $48h_2$ and $48h_3$ sites, respectively, in the semiclathrate structure. Atoms in the $48h_3$ site (small black circles) remain three-bonded. If there are vacancies in the guest positions, some of the atoms in the $48h_2$ sites also become three-bonded (right).

Scheme 1. Splitting of Wyckoff Sites upon Transformation from the Space Group $Pm\bar{3}n$ to $Fm\bar{3}$

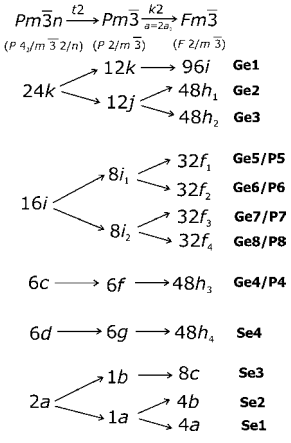

Table 3. Selected Interatomic Distances (Å) for $[Ge_{46-x}P_x]Se_{8-y}\square_y$

	I	II	II (173 K)
Se(4)−Ge(3)	2.242(2)	2.3287(8)	2.3229(6)
Ge(1)−E(4)[a]	2.332(1)	2.3449(9)	2.3409(6)
Ge(1)−E(7)	2.3877(9)	2.3945(6)	2.3865(4)
Ge(1)−E(6)	2.3934(9)	2.4016(5)	2.3954(4)
Ge(1)−Ge(1)	2.437(1)	2.4471(8)	2.4395(5)
Ge(2)−E(4)	2.362(3)	2.367(1)	2.361(1)
Ge(2)−E(8)	2.3882(9)	2.3969(6)	2.3909(4)
Ge(2)−Ge(2)	2.463(1)	2.475(1)	2.4692(7)
Ge(3)−E(5)	2.369(1)	2.3691(6)	2.3637(5)
Ge(3)−Ge(3)	2.461(1)	2.454(1)	2.4448(7)
E(5)−E(6)	2.332(3)	2.337(1)	2.328(1)
E(7)−E(8)	2.310(3)	2.314(1)	2.310(1)

[a]E4= (Ge4)/(P4); E5= (Ge5)/(P5); E6= (Ge6)/(P6); E7= (Ge7)/(P7); E8= (Ge8)/(P8).

only because of the rearrangement of atoms of the framework (Figure 3).

5. Superstructure by Electron Microscopy. Selected area electron diffraction (SAED) proves the presence of the superstructure. Diffraction patterns for structure **II** indicate an *F*-centered cubic cell with $a \approx 20.4$ Å (Figure 4). No additional systematic extinctions, except those corresponding to the face-centered cubic lattice, were observed, confirming the choice of the space group.

High-resolution HAADF STEM images were taken along [100] (Figure 5, top) and [110] (Figure 5, bottom) directions. On HAADF STEM images, projected atomic columns appear as dots of different brightness, roughly proportional to Z^n (n = 1−2, Z is the average atomic number along the column). The images demonstrate the structure free from planar defects. Theoretical images calculated by using the determined crystal structure **II** are in excellent agreement with the experimental images that evidence a proper structure solution. Because of the complexity of the structure a straightforward assignment of the atomic columns on the HAADF-STEM images is difficult. A figure with the most pronounced structure details superimposed on the experimental HAADF-STEM images is presented in Figure 6.

6. Relationships to Other Clathrates. One of the most intriguing features of $[Ge_{46-x}P_x]Se_{8-y}\square_y$ is a covalent bond between the guest selenium atoms and the framework. The same is also true for $[Ge_{46-x}P_x]Te_y$, where tellurium atoms act as guests. However, in analogous silicon-based compound $[Si_{46-x}P_x]Te_y$ all guest tellurium atoms are completely isolated and there is no evidence for the presence of covalent bonds formed with the framework atoms. Strong interactions between

dx.doi.org/10.1021/ic3011025 | Inorg. Chem. 2013, 52, 577−588

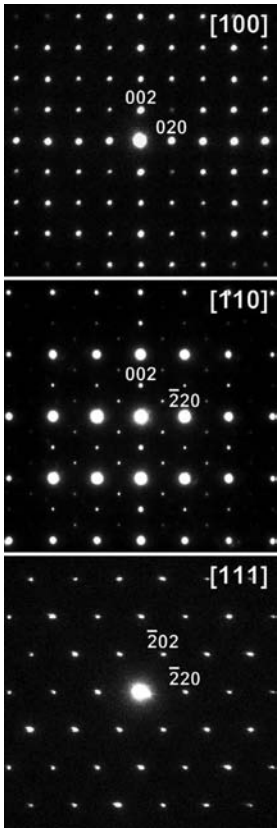

Figure 4. SAED patterns of $Ge_{30.6}P_{15.4}Se_8$.

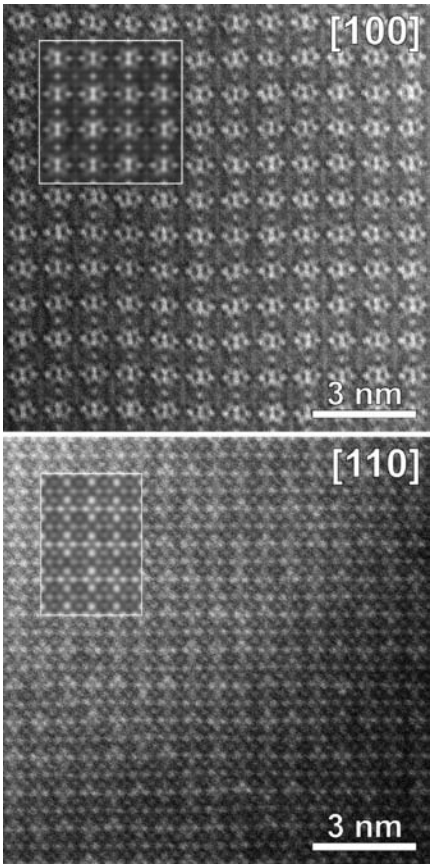

Figure 5. HAADF-STEM images of [100] and [110] zones for $Ge_{30.6}P_{15.4}Se_8$ along with the simulated images (shown as inserts) for $Ge_{30.6}P_{15.4}Se_8$.

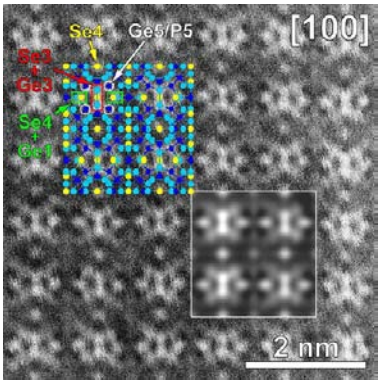

Figure 6. The simulated [100] image and the [100] projection of the unit cell are superimposed on the experimental image for $Ge_{30.6}P_{15.4}Se_8$. Marked atomic columns cause the most pronounced details to the image. Both simulation and structure image are of the size of one unit cell.

the host and guest substructures were reported for the rhombohedral modification of $[Si_{38}Te_8]Te_8$, where d(Te2–Si33) = 2.63 Å.[15] This distance is longer than the typical length of the Si–Te bond (2.58 Å in Si_2Te_3[28] and 2.50 Å in Ba_2SiTe_4[29]), but it is comparable with the interatomic Si–Te distances within the framework (2.589–2.798 Å). Evidently, the reason for the short distance between the guest atoms and the framework is not in the dimensional factor, because $[Si_{46-x}P_x]Te_y$ has one of the smallest unit cell parameters among all clathrates (Table 4). Actually, the effective volume of the large cages seems to be the most important characteristic. But even in that case, this value is the smallest for $[Si_{46-x}P_x]Te_y$. Moreover, no kind of strong interaction is observed for halide-based cationic clathrates, in spite of the fact that some of them have rather small 24-vertex cavities, for example, $Si_{40}P_6I_{6.5}$.[13]

In the case of $[Ge_{46-x}P_x]Se_{8-y}\square_y$ and $[Ge_{46-x}P_x]Te_y$ the formation of the covalent bond between the selenium/tellurium guest and the framework atoms is associated with the reconstruction of the framework, leading to the superstructure without the formation of vacancies within the framework. The supercell in some anionic clathrates, such as $Ba_8Ge_{43}\square_3$[30] and $Rb_8Sn_{44}\square_2$,[31] exists due to the partial or complete ordering of vacancies within the framework. These compounds crystallize in the space group $Ia\bar{3}d$ with the 8-time increase in the unit cell volume. Another type of superstructure is realized in $[Sn_{14}In_{10}P_{21.2}\square_{0.8}]I_8$ ($P4_2/m$, No. 84),[12b] where a particular arrangement of vacancies allows the mixed occupancy of the same framework position by three-bonded and four-bonded tin atoms to be avoided. In the crystal structure of $[Si_{46-x}P_x]Te_y$ vacancies arrange in the guest positions and cause lowering of the symmetry from the space group $Pm\bar{3}n$ to $Pm\bar{3}$ without a change in the unit cell dimensions.[14a] All mentioned types of superstructure appear due to vacancy ordering either in the framework or guest positions. In semiclathrate $[Ge_{46-x}P_x]Se_{8-y}\square_y$ there are also vacancies in guest positions, but they have no influence on the superstructure formation.

7. Electronic Structure and Bonding. Quantum chemical calculations and analysis of chemical bonding were made in order to get more information on the atomic interactions. The calculations were performed for the ordered model $Ge_{32}P_{14}Se_8$, that closest to the experimentally found composition $Ge_{30.54}P_{15.46}Se_{7.97}$. One of the possible ordering variants yielding

dx.doi.org/10.1021/ic3011025 | Inorg. Chem. 2013, 52, 577–588

Table 4. Unit Cell Parameters and Volume of Guest Cavities, Calculated for the Inner Spheres, for Selected Si- and Ge-Based Cationic Clathrates-I

compd	unit cell parameter, Å	normalized unit cell vol, Å^3	vol of a [5^{12}] cage, Å^3	vol of a [$5^{12}6^2$] cage, Å^3	ref
$Si_{31.3}P_{14.7}Te_{7.4}$	9.976	992.82	95.6	133.6	14a
$Si_{40}P_6I_{6.5}$	10.1293	1039.29	97.96	140.56	13
$Ge_{30.54}P_{15.46}Se_{7.97}$[a]	20.406	1062.15	106.93	141.38	*b*
$Ge_{30.40}P_{15.60}Te_{5.92}$[a]	20.544	1083.84	110.02	143.97	17
$Ge_{38}P_8I_8$	10.4983	1157.06	111.25	155.76	11

[a]In $Ge_{30.54}P_{15.46}Se_{7.97}$ and $Ge_{30.40}P_{15.60}Te_{5.92}$ larger cages cannot be simply described in polyhedral presentation corresponding to the formulas [$5^{12}6^2$]. [b]This work.

the composition $Ge_{32}P_{14}Se_8$ was chosen; the occupation of the atomic positions is given in Table 5.

Table 5. Electron Density Analysis for $Ge_{32}P_{14}Se_8$

position	basin vol, Å^3	basin population, e$^-$	QTAIM charge
Se1, 4*a* site	24.72	35.22	−1.22
Se2, 4*b* site	24.48	34.97	−0.97
Se3, 8*c* site	24.62	35.15	−1.15
Se4, 48*h* site	26.68	34.93	−0.93
Ge1, 96*i* site	15.90	31.51	+0.49
Ge2, 48*h* site	16.52	31.80	+0.20
Ge3, 48*h* site	14.61	31.30	+0.70
P4, 48*h* site	21.03	15.80	−0.80
P5, 32*f* site	18.13	15.13	−0.13
Ge6, 32*f* site	17.49	32.13	−0.13
Ge7, 32*f* site	16.64	31.83	+0.17
P8, 32*f* site	17.69	15.08	−0.08

In general, the interaction between the framework and the filler atoms in intermetallic clathrates is understood as an ionic one. In anionic clathrates, the filler atoms deliver their valence electrons for the fulfilling of the electronic requirements of the framework atoms and forming covalent bonds within the framework. This picture is reflected in the electronic density of states by formation of the gap and filling of the bonding states below the Fermi level. The case with the reversed host−guest polarity is true for $Ge_{32}P_{14}Se_8$, where the fillers accept electrons from the framework atoms. It is not surprising that the calculated electronic density of states reflects the formal Zintl counting $[(4b)Ge^0]_{32}[(4b)P^{1+}]_{14}[(0b)Se^{2-}]_8 \cdot 2\square^+$ (where 4*b*, 2*b*, and 0*b* stand for four-connected, two-connected, and isolated atoms, respectively) which does not account for the special situation around the Se4 position. Namely, the bonding states are slightly underoccupied, meaning that a gap of ca. 0.9 eV forms above the Fermi level (Figure 7). The whole DOS is formed mainly by *s* and *p* states of Ge and P—the *s* and *p* states of selenium contribute to all energy ranges proportional to the multiplicity of the crystallographic sites. The structurally unique Se4 (single-bonded to the Ge3) differs solely in the region between −12 and −11 eV, where it contributes stronger than the nonconnected selenium atoms, reflecting the transformation of the nonbonding states in the isolated species to the bonding ones in Se4 (Figure 7, top). Contributions of all Ge position are present in a wide range of energies below the Fermi level, independently on the interaction of Ge3 with Se4 (Figure 7, bottom). The Ge(*p*) states form the sharp maximum of DOS at the Fermi level, which is one of the reasons of the high thermoelectric power (Seebeck coefficient)[3] observed experimentally (cf. below). As expected from the structural picture, the three-connected position P4 contributes very

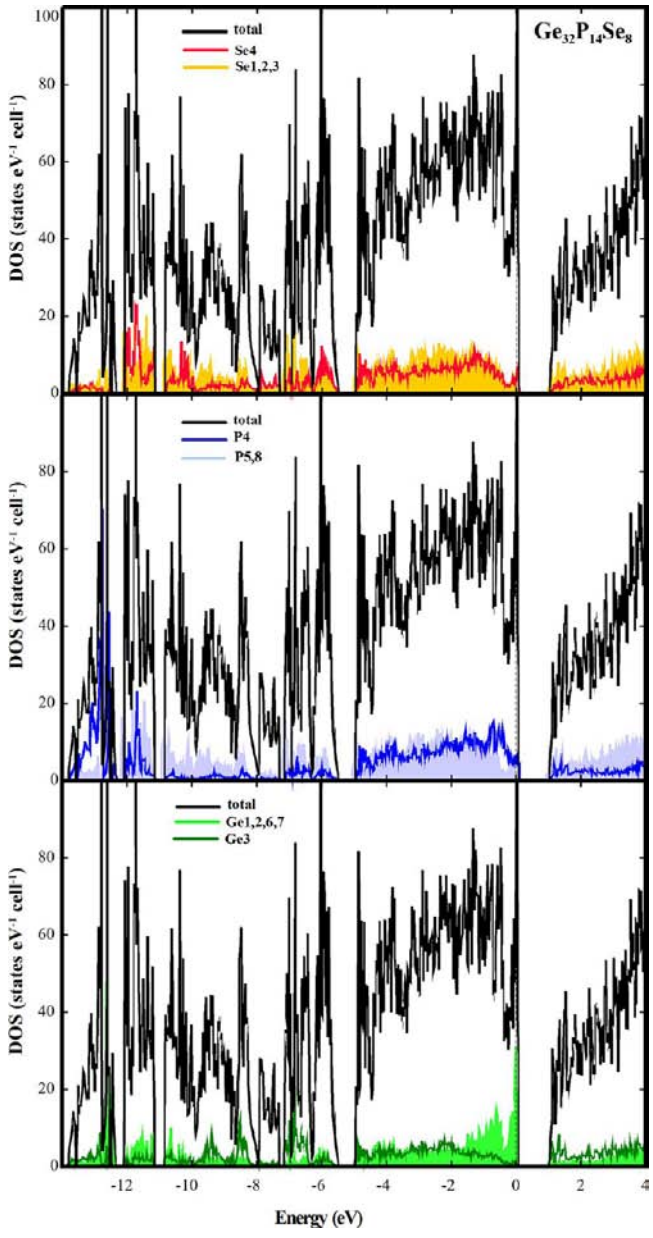

Figure 7. Electronic density of states for the model with composition $Ge_{32}P_{14}Se_8$. E_F is set as 0 eV.

strongly in the range below −12.5 eV, reflecting the formation of the lone pair at this position in contrast to the four-connected atoms P5 and P8 (Figure 7, middle).

Further understanding of the role of different elements in the structure, especially about their charges, was obtained by the analysis of the calculated electron density in accordance with

dx.doi.org/10.1021/ic3011025 | *Inorg. Chem.* 2013, 52, 577−588

the Quantum Theory of Atoms In Molecules (QTAIM) of Bader.[25] The volumes of the QTAIM basins of Se1, Se2, and Se3 are markedly larger than that of Se4 (Table 5). The atomic basins of the isolated positions of Se1−Se3 have similar volumes, and the volume of the Se4 species is the largest one. Integration of the electron density within these basins yields the according charges. In contrast to the tendency in the volume change, the basins of all selenium positions reveal similar charges independent of the difference in the number of closest contacts: (1*b*)Se4 vs (0*b*)Se1−Se3. All Se positions show negative charges as expected from the electronegativity of the elements *EN*(Se) > *EN*(P) > *EN*(Ge). Among the phosphorus positions the three-connected site P4 has the largest volume and the largest charge, reflecting the formation of the lone pair at this position. Germanium atoms Ge1, Ge2, Ge3, and Ge7 have positive charges in agreement with the electronegativity ratio. Thereby Ge3 shows the largest charge and the smallest volume reflecting its direct interaction with the more electronegative Se4. The slightly negative charge on the Ge6 site hints for a possible occupation of this position with the more electronegative phosphorus, which goes along with the opposite tendency in the occupation of position P8. Following the QTAIM charges, selenium is the most electropositive element and plays the role of the anions. Germanium and phosphorus have positive and negative QTAIM charges, respectively. Thus the Ge−P bonding should be a polar one, whereby the whole framework is a polycation due to the prevalent positive charges of Ge.

To complete the bonding picture, the topology electron localizability indicator was analyzed. The distribution of the ELI-D reveals maxima between the germanium and phosphorus as well as between germanium atoms (Figure 8, top) and

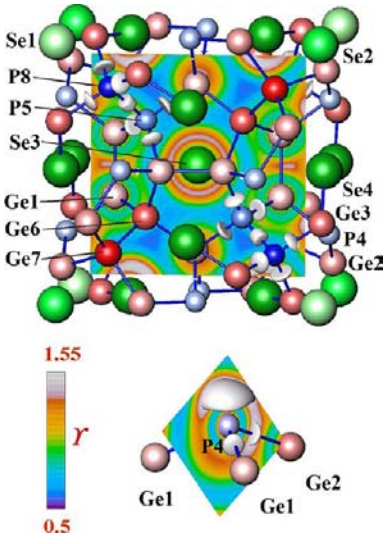

Figure 8. Electron localizability indicator for the model with composition $Ge_{32}P_{14}Se_8$.

confirms the direct covalent bonding within the framework. As obtained by the combined analysis of the electron density and ELI-D by means of the so-called basin intersection technique,[32] the contribution of the QTAIM basins of the phosphorus atoms to the charge of the Ge−P bonding basins in ELI-D is much larger than that of the QTAIM Ge basins. This finding finally confirms a picture of the polar covalent interactions between P and Ge atoms within the framework. The distribution of ELI-D around the P4 nucleus reveals three maxima on the Ge−P contacts visualizing the two-center Ge−P bonds. The ELI-D maximum on the bond-opposite site of the nucleus is in contact only with one core basin, thus revealing the formation of a "lone-pair" (Figure 8, bottom).

The ELI-D distribution of the selenium species shows four shells. For Se1−Se3 the ELI-D distribution in the outer (4th) shells is very close to a spherical one. The structuring in these shells, which may indicate a participation of the electrons of these shells in the bonding,[33] is minimal (Figure 8, top). No ELI maxima were found between these Se species and the framework atoms. In contrast to that, the fourth shell of the Se4 species reveals a very strong structuring. A maximum of ELI-D is formed on the Ge3−Se4 contact visualizing here the directed bond (4b)Ge3−(1b)Se4 (Figure 9, top). On the bond-opposite

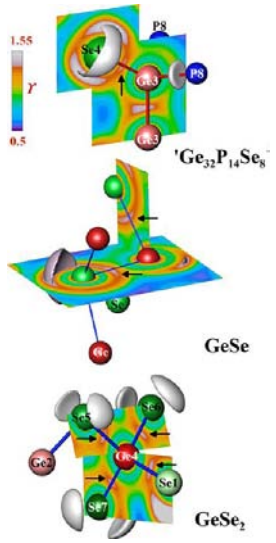

Figure 9. Se−Ge bonding in $Ge_{32}P_{14}Se_8$ in comparison with GeSe and $GeSe_2$.

side a formation of the "lone-pair"-like maxima is observed. Practically identical ELI-D distributions are observed for the (3b)Ge−(3b)Se with *d*(Ge−Se) of 2.56−2.57 Å and (4b)Ge−(2b)Se with *d*(Ge−Se) = 2.35−2.38 Å in GeSe[34] and $GeSe_2$,[35] respectively.

Thus the atomic interactions in $Ge_{32}P_{14}Se_8$ can be summarized as follows. The cationic framework is formed by covalent Ge−Ge and polar covalent Ge−P bonds. Coulomb interactions were found between the Se anions and the framework. In addition, direct covalent bonds are found between framework atom Ge3 and filler species Se4. Formation of this bond causes breaking one of the bonds within the framework and leads to formation of lone electron pairs on the adjacent (phosphorus) atoms.

The formation of the covalent bonding between the framework and the filler species without the strong shifts in both substructures was observed in the intermetallic clathrate $Ba_8Au_{5.3}Ge_{40.7}$ (Ba−Au interaction).[36] In the filled skutterudite $Sn_xPt_4Sn_ySb_{12-y}$, the Sn−Sb bonding leads to the shift of the filler atom from the center of the cavity, where it is located.[37] In the case of the clathrate Ba_6Ge_{25}, the formation of the covalent Ba−Ge bonds leads at low temperature to a structural transition caused by the breaking of the Ge−Ge bonds within the framework.[38] Observation of the host−guest interaction with

dx.doi.org/10.1021/ic3011025 | *Inorg. Chem.* 2013, 52, 577−588

and without the shift of a guest atom away from the cage center makes a strict definition of semiclathrates difficult.

8. Electron Counting and Transport Properties. The Zintl counting scheme is applicable for prediction and explanation of transport properties of many semiconducting clathrates, including those having the reversed polarity.[10,39] In this work, it was used for calculating the charge balance for structures **I** and **II**, assuming the following structural details. For both structures the Ge/P ratio is almost the same and equals 30.6/15.4. However, upon varying the selenium content the Ge/P ratio for an individual position changes, leading to the different occupancy of the 3-coordinated and 4-coordinated positions by phosphorus and germanium atoms. Within the Zintl electron counting scheme, each atom completes its 8-electron configuration by forming two-center, two-electron bonds and (if necessary) by forming lone electron pairs. According to this, each four-bonded phosphorus atom is assigned a formal charge of +1 and each three-bonded germanium atom is assigned a formal charge of −1, whereas all the rest of the atoms of the framework are formally uncharged. In a similar way selenium atoms with one host−guest bond have a formal charge of −1 and those without bonds are assigned a formal charge of −2. Following this scheme, we calculated the electronic balance for structures **I** and **II** and found a small residual negative charge of −0.3 to 0.4 per formula for both structures. Similar imbalance was calculated for semiclathrates of the Ge−P−Te system[17] and type-I clathrates of the Si−P−Te system;[14a] the imbalance is small and only slightly exceeds the esd threshold, therefore no reliable prediction of the transport properties can be made.

Measurements of the electrical conductivity and Seebeck coefficient were carried out only for the $Ge_{30.6}P_{15.4}Se_8$ sample in the temperature range of 300−673 K. Thermal behavior of the electrical resistivity corresponds to that of a typical semiconductor (Figure 10 top). This differentiates $Ge_{30.6}P_{15.4}Se_8$ from silicon clathrates $Si_{32.5}P_{13.2}Te_{6.65}$ and $Si_{32.00}P_{14.10}Te_{7.25}$,[14a,e] which also feature slight deviation from the Zintl scheme but demonstrate temperature dependences of the electrical conductivity typical for heavily doped semiconductors or semimetals (Table 6). The electrical conductivity σ is of the activation type, $\sigma \approx \exp(-E_a/2kT)$, where E_a is the activation energy, k is the Boltzmann constant, and T is the absolute temperature. From linearization of the $\ln(\sigma)$ versus T^{-1} function (Figure 10, bottom) the band gap was estimated to be 0.41 eV, being of the same order of magnitude as 0.9 eV calculated for model $Ge_{32}P_{14}Se_8$. This value is smaller than those reported for $Ge_{30}P_{16}Te_8$ (0.62 eV)[16] and $Ge_{38}Sb_8I_8$ (1.16 eV)[12e] but larger than for $Ge_{38}P_8I_8$ (0.34 eV) and $Ge_{38}As_8I_8$ (0.24 eV).[11b]

The Seebeck coefficient (Figure 11, top) is negative in the whole temperature range, indicating that electrons are the major charge carriers, and rises in absolute value on heating (in agreement with the shape of calculated electronic density of states), reaching the maximal absolute value of $S = 525\ \mu V\ K^{-1}$. There are other examples of cationic clathrates with negative values of the Seebeck coefficient, for instance, $Ge_{38}Sb_8I_8$ (−800 $\mu V\ K^{-1}$ at 300 K and −600 $\mu V\ K^{-1}$ at 750 K),[12e] $Sn_{38}Sb_8I_8$ (−600 $\mu V\ K^{-1}$ at 300 K and −500 $\mu V\ K^{-1}$ at 550 K),[12] and $Sn_{20.5}\square_{3.5}As_{22}I_8$ (−180 $\mu V\ K^{-1}$ at 300 K)[12d] (Table 6).

For a thermoelectric material, the power factor PF defined as a product of the electrical conductivity and squared Seebeck coefficient expresses the efficiency of the charge carrier's transport. The temperature dependence of the power factor is given in Figure 11 (bottom). The maximum value reaches approximately 2.3×10^{-5} W K^{-2} m^{-1} at 660 K, which is comparable with that for $Ge_{30}P_{16}Te_8$ and $Ge_{38}Sb_8I_8$ (20 and 2.1×10^{-5} W K^{-2} m^{-1}, respectively).[12f,16] Although quite low values of the thermal conductivity κ are expected for $Ge_{30.6}P_{15.4}Se_8$, the dimensionless thermoelectric figure-of-merit defined as $ZT = PF\ T\kappa^{-1}$ is expected to be below 0.03 at 660 K.

Investigation of the thermal conductivity and specific heat of the selenium semiclathrates is currently in progress.

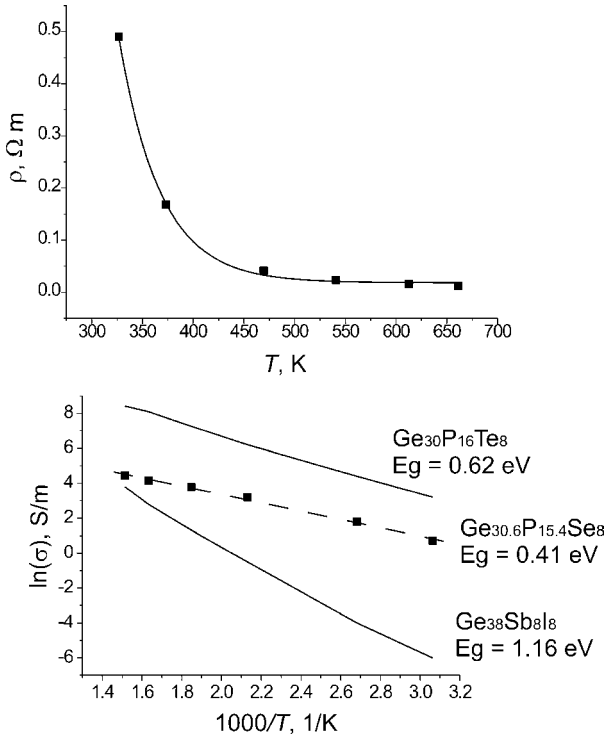

Figure 10. (top) Temperature dependences of the electrical resistivity ρ for $Ge_{30.6}P_{15.4}Se_8$; solid line is drawn to guide the eye. (bottom) A $\ln(\sigma)$ versus T plot for $Ge_{30.6}P_{15.4}Se_8$ in comparison with other cationic clathrates. Dashed line is a linear fit. The data for $Ge_{30}P_{16}Te_8$[16] and $Ge_{38}Sb_8I_8$,[12f] are taken from the literature, shown as solid lines.

Table 6. Physical Properties of Si- and Ge-Based Cationic Clathrates-I

clathrates	resistivity (Ohm m) at 300 K	Seebeck coefficient ($\mu V\ K^{-1}$) at 300 K	ref
$Ge_{30.6}P_{15.4}Se_8$	4.9×10^{-1} (at 325 K)	−200	*a*
$Ge_{30}P_{16}Te_8$	3.16×10^{-1}	750	16
$Si_{32.8}P_{13.3}Te_{6.70}$	2.5×10^{-4}		14e
$Si_{32.1}P_{14.1}Te_{7.25}$	10^{-3}		14e
$Si_{46-x}P_xTe_8$ ($11 \le x \le 17$)	2×10^{-5} ($x = 11$) $\le \rho \le$ 63.3 ($x = 17$)	60 ($x = 11$) $\le S \le$ 220 ($x = 15$)	14b
$Ge_{38}Sb_8I_8$	1000	−800	12e

[a]This work.

■ CONCLUSIONS

New cationic type-I related clathrate $[Ge_{46-x}P_x]Se_{8-y}\square_y$ (x = 15.4(1); y = 0−2.65) was prepared from the elements. Its crystal structure reveals two important features. The unit cell parameter is doubled compared with that of the usual clathrate-I pattern. The superstructure is caused by the reconstruction of the cationic framework, leading to the appearance of three-bonded atoms without vacancy formation. $[Ge_{46-x}P_x]Se_{8-y}\square_y$

dx.doi.org/10.1021/ic3011025 | *Inorg. Chem.* 2013, 52, 577−588

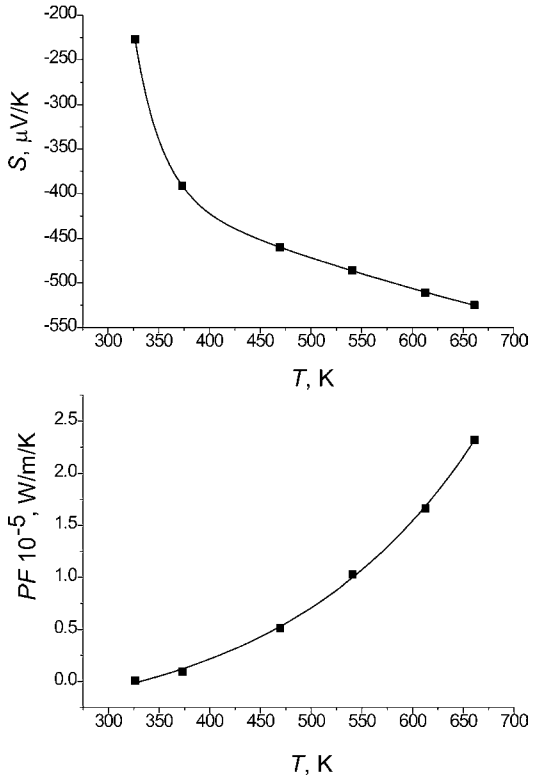

Figure 11. Temperature dependences of the Seebeck coefficient *S* (top) and power factor PF (bottom) for $Ge_{30.6}P_{15.4}Se_8$. Solid lines are drawn to guide the eye.

stands apart from other compounds with a superstructure of the clathrate-I type, where the superstructure arises from the partial or full vacancy ordering.

The cationic framework is formed by covalent Ge−Ge and polar covalent Ge−P bonds. Coulomb interactions were found between the Se anions and the framework. In addition, direct covalent bonds are found between the framework Ge atoms and part of the filler Se species.

The results of measurements of transport properties are in agreement with the Zintl counting scheme and the calculated electronic density of states. The cationic clathrate $[Ge_{46-x}P_x]Se_{8-y}\square_y$ is the *n*-type semiconductor with the estimated band gap of 0.41 eV for $y = 0$. The title compound displays high values of the Seebeck coefficient but rather low electrical conductivity. Combined, this leads to moderate values of the thermoelectric power factor with the maximum of 2.3×10^{-5} W K^{-2} m^{-1} at 660 K, which means that doping aiming at achieving lower electrical resistivity is necessary for attaining promising thermoelectric performance.

■ ASSOCIATED CONTENT

Supporting Information

X-ray crystallographic data for $[Ge_{46-x}P_x]Se_{8-y}\square_y$ in CIF format, DSC curve for $Ge_{30.6}P_{15.4}Se_8$. This material is available free of charge via the Internet at http://pubs.acs.org.

■ AUTHOR INFORMATION

Corresponding Author

*E-mail: shev@inorg.chem.msu.ru. Tel.: (+7-495) 939 33 39. Fax: (+7-495) 939 47 88.

Present Address

#Department of Chemistry, University of California, Davis, 95616 California.

Notes

The authors declare no competing financial interest.

■ ACKNOWLEDGMENTS

The authors thank Dr. S. Y. Istomin for the thermal analysis and Mr. V. Y. Verchenko for the EDX analysis, as well as Dr. M. Kohout and Dr. F. R. Wagner for discussions on chemical bonding. M.A.K. thanks the MSU-NIMS bilateral program for supporting her stay at NIMS. This work was supported in part by the Lomonosov Moscow State University Program of Development and the Russian Foundation for Basic Research.

■ REFERENCES

(1) Jeffrey, G. A. in *Inclusion Compounds*; Atwood, J. L., Davies, J. E. D., MacNicol, D. D., Eds.; Academic Press Inc.: London, UK, 1984.

(2) Kasper, J. S.; Hagenmuller, P.; Pouchard, M.; Cros, C. *Science* **1965**, *150*, 1713−1714.

(3) Slack, G. A. in *CRC Handbook of thermoelectrics*; Rowe, D. M., Ed.; Chemical Rubber: Boca Raton, FL, 1995; Vol. 2, p 407.

(4) (a) Nolas, G. S.; Cohn, J. L.; Slack, G. A.; Schujman, S. B. *Appl. Phys. Lett.* **1998**, *73*, 178−180. (b) Saramat, A.; Svensson, G.; Palmqvist, A. E. C.; Stiewe, C.; Mueller, E.; Platzek, D.; Williams, S. G. K.; Rowe, D. M.; Bryan, J. D.; Stucky, G. D. *J. Appl. Phys.* **2006**, *99* (023708), 1−5.

(5) (a) Yamanaka, S.; Enishi, E.; Fukuoka, H.; Yasukawa, M. *Inorg. Chem.* **2000**, *39*, 56−58. (b) Fukuoka, H.; Kiyoto, J.; Yamanaka, S. *J. Solid State Chem.* **2003**, *175*, 237−244. (c) Fukuoka, H.; Kiyoto, J.; Yamanaka, S. *Inorg. Chem.* **2003**, *42*, 2933−2937. (d) Fukuoka, H.; Kiyoto, J.; Yamanaka, S. *J. Phys. Chem. Solid* **2004**, *65*, 333−336.

(6) Paschen, S.; Carrillo-Cabrera, W.; Bentien, A.; Tran, V. H.; Baenitz, M.; Grin, Y.; Steglich, F. *Phys. Rev. B* **1999**, *64* (214404), 1−11.

(7) Kawaguchi, T.; Tanigaki, K.; Yasukawa, M. *Appl. Phys. Lett.* **2000**, *77*, 3438−3440.

(8) Shevelkov, A. V.; Kovnir, K. A. *Struct. Bonding (Berlin)* **2011**, *139*, 97−144.

(9) Kirsanova, M. A.; Olenev, A. V.; Abakumov, A. M.; Bykov, M. A.; Shevelkov, A. V. *Angew. Chem., Int. Ed.* **2011**, *50*, 2371−2374.

(10) *Chemistry, Structure and Bonding of Zintl Phases and Ions*; Kauzlarich, M. S., Ed.; VCH Publishers: New York, NY, 1996.

(11) (a) von Schnering, H. G.; Menke, H. *Angew. Chem., Int. Ed.* **1972**, *11*, 43−44. (b) Menke, H.; von Schnering, H. G. *Z. Anorg. Allg. Chem.* **1973**, *395*, 223−238.

(12) (a) Shatruk, M. M.; Kovnir, K. A.; Shevelkov, A. V.; Presniakov, I. A.; Popovkin, B. A. *Inorg. Chem.* **1999**, *38*, 3455−3457. (b) Kovnir, K. A.; Shatruk, M. M.; Reshetova, L. N.; Presniakov, I. A.; Dikarev, E. V.; Baitinger, M.; Haarmann, F.; Schnelle, W.; Baenitz, M.; Grin, Y.; Shevelkov, A. V. *Solid State Sci.* **2005**, *7*, 957−968. (c) Zaikina, J. V.; Kovnir, K. A.; Sobolev, A. V.; Presniakov, I. A.; Prots, Y.; Baitinger, M.; Schnelle, W.; Olenev, A. V.; Lebedev, O. I.; Van Tendeloo, G.; Grin, Y.; Shevelkov, A. V. *Chem.—Eur. J.* **2007**, *13*, 5090−5099. (d) Kovnir, K. A.; Sobolev, A. V.; Presniakov, I. A.; Lebedev, O. I.; Van Tendeloo, G.; Schnelle, W.; Grin, Y.; Shevelkov, A. V. *Inorg. Chem.* **2005**, *44*, 8786−8793. (e) Kishimoto, K.; Arimura, S.; Koyanagi, T. *Appl. Phys. Lett.* **2006**, *88* (222115), 1−3.

(13) (a) Kovnir, K. A.; Uglov, A. N.; Zaikina, J. V.; Shevelkov, A. V. *Mendeleev Commun.* **2004**, *4*, 135−136. (b) Reny, E.; Yamanaka, S.; Cros, C.; Pouchard, M. *Chem. Commun.* **2000**, 2505−2506.

(14) (a) Zaikina, J. V.; Kovnir, K. A.; Schwarz, U.; Borrmann, H.; Shevelkov, A. V. *Z. Kristallogr.-New Cryst. Struct.* **2007**, *222*, 177−179. (b) Kishimoto, K.; Koyanagi, T.; Akai, K.; Matsuura, M. *Jap. J. Appl. Phys., Part 2* **2007**, *46*, L746−L748. (c) Philipp, F.; Schmidt, P. *J. Cryst. Growth* **2008**, *310*, 5402−5408. (d) Zaikina, J. V.; Kovnir, K. A.; Burkhardt, U.; Schnelle, W.; Haarmann, F.; Schwarz, U.; Grin, Y.;

Shevelkov, A. V. *Inorg. Chem.* **2009**, *48*, 3720−3730. (e) Zaikina, J. V.; Mori, T.; Kovnir, K.; Teschner, D.; Senyshyn, A.; Schwarz, U.; Grin, Yu.; Shevelkov, A. V. *Chem.—Eur. J.* **2010**, *16*, 12582−12589.
(15) (a) Jaussaud, N.; Toulemonde, P.; Pouchard, M.; San Miguel, A.; Gravereau, P.; Pechev, S.; Goglio, G.; Cros, C. *Solid State Sci.* **2004**, *6*, 401−411. (b) Jaussaud, N.; Pouchard, M.; Gravereau, P.; Pechev, S.; Goglio, G.; Cros, C.; San Miguel, A.; Toulemonde, P. *Inorg. Chem.* **2005**, *44*, 2210−2214.
(16) Kishimoto, K.; Akai, K.; Muraoka, N.; Koyanagi, T.; Matsuura, M. *Appl. Phys. Lett.* **2006**, *89* (172106), 1−3.
(17) Kirsanova, M. A.; Reshetova, L. N.; Olenev, A. V.; Abakumov, A. M.; Shevelkov, A. V. *Chem.—Eur. J.* **2011**, *17*, 5719−5726.
(18) Shatruk, M. M.; Kovnir, K. A.; Lindsjo, M.; Presniakov, I. A.; Kloo, L. A.; Shevelkov, A. V. *J. Solid State Chem.* **2001**, *161*, 233−242.
(19) Sheldrick, G. M. *Acta Crystallogr., Sect. A* **2008**, *64*, 112−122.
(20) Koch, C. Ph.D. Thesis, Arizona State University, Phoenix, AZ, 2002.
(21) Jepsen, O.; Burkhardt, A.; Andersen, O. K. The Program TB-LMTO-ASA, Version 4.7, Max-Planck-Institut für Festkörperforschung, Stuttgart, 1999.
(22) von Barth, U.; Hedin, L. *J. Phys. C: Solid State Phys.* **1972**, *5*, 1629−1642.
(23) Andersen, O. K. *Phys. Rev. B: Condens. Matter Mater. Phys.* **1975**, *12*, 3060−3083.
(24) (a) Kohout, M. *Int. J. Quantum Chem.* **2004**, *97*, 651−658. (b) Kohout, M.; Wagner, F. R.; Grin, Yu. *Int. J. Quantum Chem.* **2006**, *106*, 1499−1507. (c) Kohout, M. *Faraday Discuss.* **2007**, *135*, 43−54.
(25) Bader, R. F. W. Atoms in Molecules, A Quantum Theory; Clarendon Press and Oxford University Press Inc.: New York, 1994.
(26) Kohout, M. DGrid, version 4.6, 2011.
(27) (a) von Schnering, H. G. *Angew. Chem.* **1981**, *93*, 44−63. (b) von Schnering, H. G.; Hönle, W. *Chem. Rev.* **1988**, *88*, 243−273.
(28) Plog, K.; Stetter, W.; Novitski, A.; Schönherr, E. *Mater. Res. Bull.* **1976**, *11*, 1147−1154.
(29) Brinknan, C.; Eisenmann, B.; Schäfer, H. *Z. Anorg. Allg. Chem.* **1985**, *524*, 83−89.
(30) (a) Carrillo-Cabrera, C.; Budnyk, S.; Prots, Yu.; Grin, Yu. *Z. Anorg. Allg. Chem.* **2004**, *630*, 2267−2276. (b) Okamoto, N. L.; Oh, M. W.; Nishii, T.; Tanaka, K.; Inui, H. *J. Appl. Phys.* **2006**, *99* (033513), 1−8. (c) Aydemir, Y.; Candolfi, C.; Borrmann, H.; Baitinger, M.; Ormeci, A.; Carrillo-Cabrera, W.; Chubilleau, C.; Lenoir, B.; Dauscher, A.; Oeschler, N.; Steglich, F.; Grin, Yu. *Dalton Trans.* **2010**, *39*, 1078−1088.
(31) (a) Dubois, F.; Fässler, T. F. *Z. Anorg. Allg. Chem.* **2004**, *630*, 1718−1718. (b) Dubois, F.; Fässler, T. F. *J. Am. Chem. Soc.* **2005**, *127*, 3264−3265.
(32) (a) Jansen, G.; Schubert, M.; Findeis, B.; Gade, L. H.; Scowen, I. J.; McPartlin, M. *J. Am. Chem. Soc.* **1998**, *120*, 7239. (b) Raub, S.; Jansen, G. *Theor. Chem. Acc.* **2001**, *106*, 223.
(33) (a) Kohout, M.; Wagner, F. R.; Grin, Yu. *Theor. Chem. Acc.* **2002**, *108*, 150−156. (b) Wagner, F. R.; Bezugly, V.; Kohout, M.; Grin, Yu. *Chem.—Eur. J.* **2007**, *13*, 5724−5741.
(34) Wiedemeier, H.; von Schnering, H. G. *Z. Kristallogr.* **1978**, *148*, 295−303.
(35) Dietmar, G.; Schäfer, H. *Acta Crystallogr.* **1976**, *32*, 2726−2728.
(36) Liang, Y.; Borrmann, H.; Baenitz, M.; Schnelle, W.; Budnyk, S.; Zhao, J.-T.; Grin, Yu. *Inorg. Chem.* **2008**, *47*, 9489−9496.
(37) Zhang, H.; Borrmann, H.; Oeschler, N.; Candolfi, C.; Schnelle, W.; Schmidt, M.; Burkhardt, U.; Baitinger, M.; Zhao, J.-T.; Grin, Yu. *Inorg. Chem.* **2011**, *50*, 1250−1257.
(38) Carrillo-Cabrera, W.; Borrmann, H.; Paschen, S.; Baenitz, M.; Steglich, F.; Grin, Yu. *J. Solid State Chem.* **2005**, *178*, 715−728.
(39) Shevelkov, A. V.; Shatruk, M. M. *Russ. Chem. Bull.* **2001**, *50*, 337−352.